Synthesis and Application of Cobalt-based Metal-organic Framework for Adsorption of Humic Acid from Water

S. Naseem,[a] Z. Aslam,[a,*] A. Abbas,[a] S. Sumbal,[a] R. Ali,[a,b] and M. Usman[c]

[a]Department of Chemical Engineering, University of Engineering and Technology, Lahore, Pakistan

[b]Department of Chemical Engineering, Khalifa University, Abu Dhabi, United Arab Emirates

[c]Chemical and Materials Engineering Department, Faculty of Engineering, King Abdulaziz University, Jeddah, Saudi Arabia

In this study, the adsorption of humic acid on cobalt based metal-organic framework (Co-MOF) was investigated. Co-MOF was synthesized via solvothermal technique and further characterized using X-ray diffraction (XRD), Fourier transform infrared spectroscopy (FTIR), and scanning electron microscopy (SEM). The characterization results of material confirm the formation of MOF structure. The adsorption kinetics, isotherms, thermodynamics, as well as isosteric heat of adsorption were also investigated by obtaining experimental adsorption data through batch experimentation. Optimum adsorption uptake of ~91 mg g^{-1} was attained at pH 6 and 305 K. Regression analysis of experimental results revealed that adsorption kinetics follows a pseudo-second-order kinetic model, and adsorption can reach equilibrium at ~20 min. Adsorption isotherm data can be well fitted with Koble Corrigan isotherm. Thermodynamic parameters demonstrated that the adsorption of humic acid is a spontaneous, endothermic, and physical process, while isosteric heat evaluations revealed the heterogeneous nature of the adsorbent. Overall, the Co-MOF was a promising choice to adsorb humic acid from water.

Keywords:
metal organic framework, humic acid, water pollution, adsorption

Introduction

A natural organic matter (NOM) is a complex mixture that comprises humic, fulvic, amino acids, and humin-like substance. NOMs may exist in surface and ground water resources, and their presence might be carcinogenic because of reaction of NOM and disinfectants. At high concentration in water, the chlorination of NOM-laden water can result in disinfection by products like trihalomethanes during the chlorination process. Other than the formation of disinfection byproducts, it augments microbial growth and ultimately increases the use of disinfectants and coagulants during water treatment processes[1]. A primary component of NOM is a macro-molecular humic acid, which is typically identified through its brownish appearance in water. It mainly contains hydroxyl, carboxyl, phenolic, and carbonyl functional groups in its aliphatic and aromatic chains. Conventional treatment of a wastewater bearing humic acid may lead to the formation of harmful compounds like haloacetonitriles, haloketones, trichloroacetaldehyde, halo acetic acids (HAAs), and trihalomethanes (THMs) as disinfection byproducts through reaction with halogens. Hence, elimination of HA from water is of great importance from an environmental and health point of view[2–4].

Several techniques like chemical coagulation[5], membrane separation[6], advanced oxidation[7], adsorption[8], and biochemical degradation[9] have been practiced to eradicate humic acid from polluted water. Among these, adsorption could be considered as the best method because of its simplicity, lack of byproducts, and most importantly, low sensitivity to toxins. Thus, different classes of materials have been reported that can effectively treat wastewater polluted with humic acid. However, most conventional materials such as zeolitic tuff[10], fly ash[11], chitosan[12], activated carbon[13], rice husk ash[14], and clay[15] show limited adsorption capacities (i.e., less than 50 mg g^{-1}). Therefore, it is required to develop an efficient adsorbent with high affinity for humic substances. Metal-organic frameworks (MOFs) is

*Corresponding author: E-mail: hmzaheer@uet.edu.pk

an innovative class of crystalline microporous materials that are available in one-, two-, and three-dimensional networks. In the development of MOFs, the choice of metal ion, ligand, synthesis route, and solvent has resulted in a variety of MOFs such as MIL, HKUST, IRMOF, UiO, Co-MOF, and ZIF[16–18].

Cobalt-based MOFs are of great importance in many areas because of their size, redox ability of cobalt metal, and nature of metal-ligand bond in the structure. Murinzi *et al.* synthesized cobalt 2-6-pyridine dicarboxylate MOF and demonstrated its successful application in electrochemical sensing[19]. Weidong Fan *et al.* described the synthesis of 2D cobalt-based metal-organic framework (UCP-32) for removal of C_3 light hydrocarbons from methane, and fuel gas purification. Results exhibit that UCP-32 has high adsorption uptake for H_2 and higher affinity for CO_2. Its narrow pore size allowed high separation selectivity for C_3 against methane[20]. The adsorptive removal of Cr(IV) (69.4 mg g^{-1}) and As(V) (71.4 mg g^{-1}) from river and wastewater samples using Co-MOF has been reported by Azile Nqombolo *et. al.* Further, they found that the prepared MOF showed good recyclability[21]. Different MOFs have been examined as propitious adsorbents for eradicating hazardous pollutants from wastewater like heavy metal cations and anions, dyes, etc., by electrostatic/hydrophobic interactions, π-π stacking, hydrogen bonding, and acid-base interactions[22–27]. However, the removal of humic acid (HA) onto MOFs has been rarely reported to date. Humic acid is a long chain molecule that contains various functional groups including –OH, –COOH, and these are present in anionic (i.e., HA–COO–) form in aqueous solution because of ionization[3,28]. The tendency of ionization of functional groups in HA suggests that the hydrogen bonding and electrostatic interactions may be proper approaches to attain highest removal efficiency of humic acid from aqueous solution.

Thus, the focus of this study was the use of cationic transition (redox active Co) metal and carboxylate linker in the synthesis of MOF that might exhibit strong positive charge surrounding the framework besides active sites formed by functional groups[29]. To ascertain the research idea, cobalt-based MOF was produced through a surfactant-assisted solvothermal method using triethylamine (TEA) as a surfactant media. The synthesized MOF material was characterized through SEM, XRD, and FTIR, and its efficacy for treatment of humic acid-bearing water was tested by batch adsorption. Isothermal, dynamic, and thermodynamic analyses were also carried out to evaluate the adsorption performance of prepared cobalt-based MOF.

Materials and methods

Chemicals

Cobalt nitrate hexahydrate $(Co(NO_3)_2 \cdot 6H_2O$, ≥99 %), dimethylformamide (DMF, 99.8 %), triethylamine (TEA, ≥99 %), and humic acid were purchased from Sigma Aldrich, United States. Dehydrated oxalic acid (99 %), hydrochloric acid (37 %), and sodium hydroxide (≥97 %) were obtained from Fisher Scientific, United States. In this study, all the chemicals were used without further purification, and distilled water was used in all the experiments.

Synthesis and characterization of cobalt-based MOF

Co-MOF was synthesized through solvothermal synthesis using the following steps. $Co(NO_3)_2 \cdot 6H_2O$ (0.70 g, 2.4 mmol), oxalic acid (0.21 g, 2.4 mmol) were dissolved in 30 mL of DMF solvent with mild stirring. TEA (0.24 g, 2.4 mmol) was added to the solution and stirred for proper mixing. Homogeneous solution was placed in a preheated oven at 120 °C for 4 h. After cooling to room temperature, pink precipitates of MOF were separated through filtration, washed with methanol to remove the unreacted substances, and dried at 40 °C for 4 h. The material was named Co-MOF. The dried Co-MOF material was examined for its morphology, crystal phases, and functional groups. Surface morphology was studied using scanning electron microscope (SU1510, Hitachi, Japan) at an accelerated voltage of 20 kV. To analyze the functional groups, Fourier transform infrared spectrometer (FTIR – 4100 type A, JASCO Inc.) was used to record the spectrum in the range of 450 to 4000 cm^{-1} using KBr pellets. X-ray powder diffraction patterns were recorded using Bruker (Germany) D8 Advance powder diffractometer to investigate the amorphous and crystalline structure of material. The analysis conditions were 20 kV voltage, 5 mA current, X-ray source of Cu Kα ($\lambda = 1.54021$ Å) operated in a 2θ range of 5° to 40° at a scan speed of 1° min^{-1}. To study the surface charge characteristics of Co-MOF, point of zero charge (PZC) was determined. For this purpose, distilled water (50 mL each) with different initial pH ranging from 2 to 10 was placed in Erlenmeyer flasks. An amount of 25 mg Co-MOF was added in each flask and left overnight on stirrer to reach equilibrium at room temperature. The equilibrium solution pH was then measured and plotted against the initial solution pH to get PZC.

Adsorption experimentation

Batch adsorption experiments were performed to study the effect of different parameters such as

initial pH, contact time, concentration, and temperature on the removal of humic acid from water. Stock solution of humic acid (HA) was prepared by dissolving 1 g of humic acid in 62.5 mL NaOH solution (0.1 M) (added to promote the complete dissolution of HA), and further adding distilled water to obtain 1 L solution. Stock solution was diluted for further experimentation. All the adsorption experiments were performed in a thermostatic shaker (150 rpm) by placing Erlenmeyer flask of 250 mL containing 50 mL HA solution and 25 mg Co-MOF. The initial solution pH (recorded using HI 8424, Hana Instruments, Italy) was adjusted using HCl or NaOH solution (0.1 M).

The effect of pH on the adsorption of HA was investigated by changing the initial pH of the HA solution from 2–10 at constant temperature of 305 K, contact time of 100 min, and HA concentration of 50 ppm. To evaluate kinetics and the equilibrium time for adsorption of humic acid, contact time was varied from 0–100 min while keeping constant HA concentration (50 ppm), temperature (305 K), and pH (6). For isotherms and thermodynamics studies, adsorption experiments were carried out by changing the HA concentration from 5 to 200 ppm at different temperatures (325 K, 305 K, 295 K, and 285 K), constant pH 6, and contact time of 100 min. After completion of each adsorption experiment, solution was filtered using Whatman filter paper No. 41. Initial and residual HA concentration was analyzed using UV-Vis spectrophotometer (Optima, SP-3000, Japan) by measuring the absorption at λ_{max} = 321 nm, and then the absorbance was compared with calibration curve (Fig. 1) to reveal the respective concentration of solution.

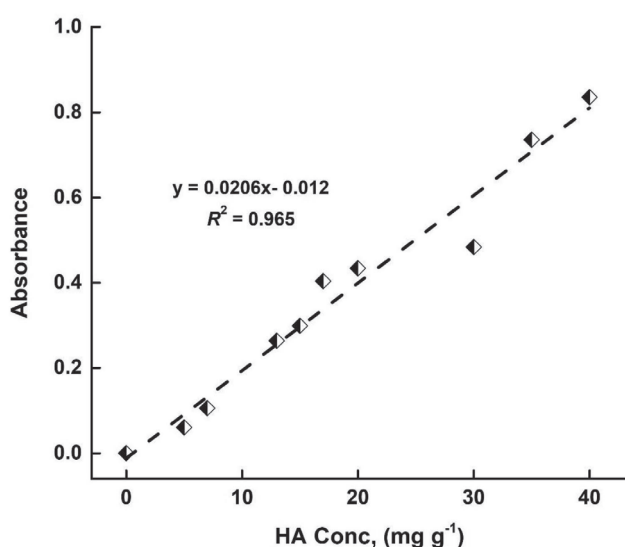Further, the uptake capacity 'q' (amount of HA adsorbed per unit mass of Co-MOF, mg g^{-1}) was evaluated using equation (1):

$$q = \frac{\left(C_0 - C_f\right)V}{m} \qquad (1)$$

where C_0 (mg g^{-1}) and C_f (mg g^{-1}) are the HA initial and final concentrations, respectively, V (L) represents the volume of humic acid solution, and m (g) is the adsorbent dosage of Co-MOF. To study the effect of various adsorption parameters and further obtain insight into the adsorption process, adsorption mechanism and thermodynamics parameters, experimental adsorption data was fitted with different kinetics and isotherm models[30–32]. The representative equations of different models are provided in Table 1.

Results and discussion

Characterization

The SEM image of synthesized Co-MOF shows well-groomed orthorhombic crystals as depicted from Fig. 2. The orthorhombic crystals of Co-MOF were further examined by XRD. Sharp diffraction peaks in the X-ray diffractograms at 7.2°, 12.4°, and 16.2° reflect the crystalline nature of MOF and respective planes of Co such as (011), (112), and (013). The intense peak at 7.2° confirms the synthesis of Co-MOF (Fig. 3)[33,34]. Furthermore, FTIR analysis was performed to study surface functional groups. Fig. 4 shows the FTIR spectra of both oxalic acid di-hydrate and Co-MOF. In spectrum of oxalic acid dihydrate, broad peak at 3466 cm^{-1} represents O–H stretching vibrations, while sharp peaks at 1638 cm^{-1} and 1475 cm^{-1} correspond to asymmetrical and symmetrical stretching vibrations of C=O bond. The adsorption peaks between 3300 cm^{-1} to 2500 cm^{-1} actually represent the O–H stretching of carboxylic acid dimers in both spectrums. Broad peak located at 3467 cm^{-1} in the Co-MOF represents O–H stretching vibrations. Absorption peaks at 1634 cm^{-1} and 1475 cm^{-1} are assigned to asymmetric and symmetric stretching vibration of C=O in the oxalic acid. In both the spectrums, peaks at 1322 cm^{-1} and 1375 cm^{-1} correspond to the bending vibrations of O–H, while the peaks at 1166 and 1156 cm^{-1} and the two bands at 1065 and 1030 cm^{-1} are assigned to C–O stretching of dicarboxylic acid, respectively. In the FTIR spectrum of oxalic acid, intensive peak at 790 cm^{-1} and intensive peak at 808 cm^{-1} appeared in the spectrum of Co-MOF, which may be assigned to out-of-plane bending motion of O–C=O functional group. Peaks at 1322 cm^{-1} and 1372 cm^{-1} correspond to the bending vibrations of C–O and O–H, respectively. Compared to FTIR spectrum of oxalic

F i g . 1 – *Calibration curve for determination of humic acid concentration*

Table 1 – *Model expressions for kinetics, isotherm, and thermodynamics studies*

| Model/Function name	Expression	Parameters/Description
Kinetics		
Pseudo first order model	$\ln(q_e - q_t) = \ln(q_e) - k_1 t$	q_e (mg g^{-1}), equilibrium adsorption uptake q_t (mg g^{-1}), instantaneous adsorption uptake k_1 (min^{-1}), pseudo first order rate constant
Pseudo second order model	$\dfrac{t}{q_t} = \dfrac{1}{k_2 q_e^2} + \dfrac{1}{q_e} t$	k_2 (g mg^{-1} min^{-1}), pseudo second order rate constant
Isotherm		
Two-parameter model		
Freundlich	$q_e = K_F C_e^{1/n_F}$	C_e (mg L^{-1}), equilibrium concentration K_F [(mg g^{-1}) (L mg)$^{1/n}$], adsorption uptake constant n_F, Freundlich parameter
Dubinin-Radushkevich	$q_e = q_{DR}\exp\left(-k_{DR}\varepsilon^2\right)$	q_{DR} (mg g^{-1}), theoretical adsorption uptake k_D (mol^2 kJ^{-2}), DR isotherm constant ε, Polanyi potential
	$E_d = \dfrac{1}{\sqrt{2k_{DR}}}$	E_d (kJ mol^{-1}), mean free energy per unit molecule of adsorbate
Three-parameter model		
Hill	$q_e = \dfrac{q_{s_H} C_e^{n_H}}{K_H + C_e^{n_H}}$	q_e (mg g^{-1}), maximum adsorption capacity K_H (mg L^{-1}), equilibrium isotherm constant n_H, Hill binding interaction parameter
Koble Corrigan	$q_e = \dfrac{A_{KC} C_e^{n_{KC}}}{1 + B_{KC} C_e^{n_{KC}}}$	A_{KC} (L^n mg^{1-n} g^{-1}) and B_{KC} (mg L^{-1}), Koble Corrigan isotherm constants n_{KC}, Koble Corrigan exponent
Thermodynamics		
Van't Hoff equation	$\Delta G^\circ = -RT \ln K$	ΔG° (kJ mol^{-1}), Gibbs free energy change R (J mol^{-1} K^{-1}), ideal gas constant T (K), absolute temperature K, distribution coefficient of adsorbent
Sorption distribution constant	$K = \dfrac{C_{ad}}{C_e}$	C_{ad} (mg g^{-1}), equilibrium concentration of adsorbate on adsorbent C_e (mg g^{-1}), equilibrium concentration of adsorbate in the solution
	$\ln K = -\dfrac{\Delta H^\circ}{R}\dfrac{1}{T} + \dfrac{\Delta S^\circ}{R}$ $\Delta G^\circ = \Delta H^\circ - T\Delta S^\circ$	ΔH° (kJ mol^{-1}), enthalpy change ΔS° (kJ mol^{-1} K^{-1}), entropy change
Clausius-Clapeyron equation	$\ln C_e = -\left(\dfrac{\Delta H_x}{R}\right)\dfrac{1}{T} + C$	ΔH_x (kJ mol^{-1}), isosteric heat of adsorption C, integration constant
Error function		
Residual sum of square	$\mathrm{RSS} = \sum_{i=1}^{n}\left(q_{e,\mathrm{cal}} - q_{e,\mathrm{exp}}\right)_i^2$	$q_{e,\mathrm{exp}}$ (mg g^{-1}), experimental adsorption uptake $q_{e,\mathrm{cal}}$ (mg g^{-1}), calculated adsorption uptake n, number of experimental data points
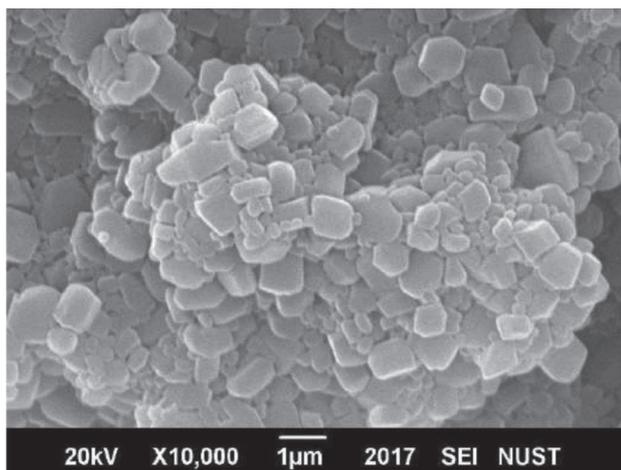
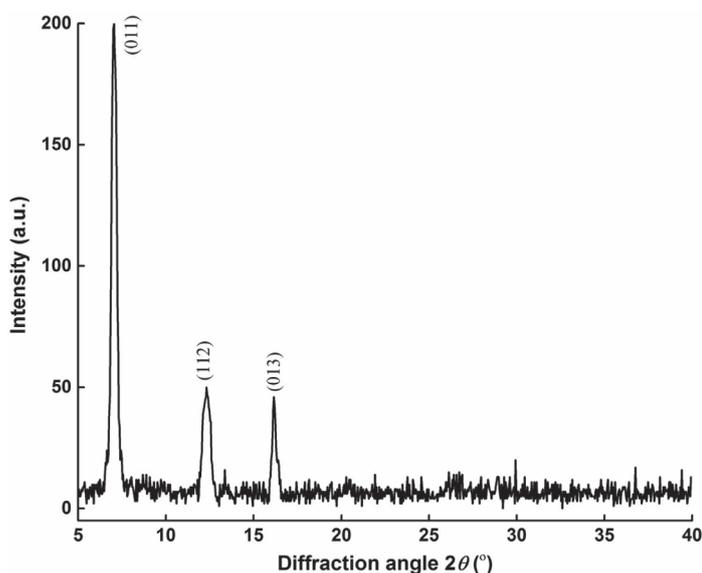Fig. 2 – *SEM image of Co-MOF*

Fig. 3 – *X-ray diffractogram of Co-MOF*

acid, an intensive peak at 808 cm^{-1} appeared in the spectrum of Co-MOF, which can be assigned to out-of-plane bending motion of O–C=O functional group and the presence of metal-oxygen bond. Small peak at low wavenumber range, i.e., 503 cm^{-1} also confirmed the bending vibration of Co–O in Co-MOF[35].

Effect of initial solution pH

The pH of pollutant solution is an important parameter, which not only affects the degree of dissociation of adsorbate but also changes the surface properties of the adsorbents. The surface charge characteristics of Co-MOF are presented in Fig. 5 as an inset graph. PZC is equivalent to ~ 7.4 corresponding to which surface is considered as neutral. Co-MOF surface has net positive charge when the pH of aqueous environment is below 7.4; however, the sorbent surface becomes net negative charged above 7.4. Based on the PZC analysis, it is evident that the adsorption of negatively charged humic acid will be favored in acidic medium over Co-MOF.

To establish the conclusion from PZC analysis, the effect of initial solution pH on the uptake of Co-MOF is presented in Fig. 5. Uptake capacity of adsorbent was different under different pH conditions. Despite negative surface of adsorbent under extreme acidic conditions, i.e., between 2 to 3 pH, low uptake capacity can be observed from Fig. 5. It can be associated to formation of oxonium ions (H$_3$O$^+$) in the solution, which decreases the dissociation of surface acidic functional groups (carboxylic and phenolic groups) present in HA. Therefore, electrostatic interactions between positively charged ad-
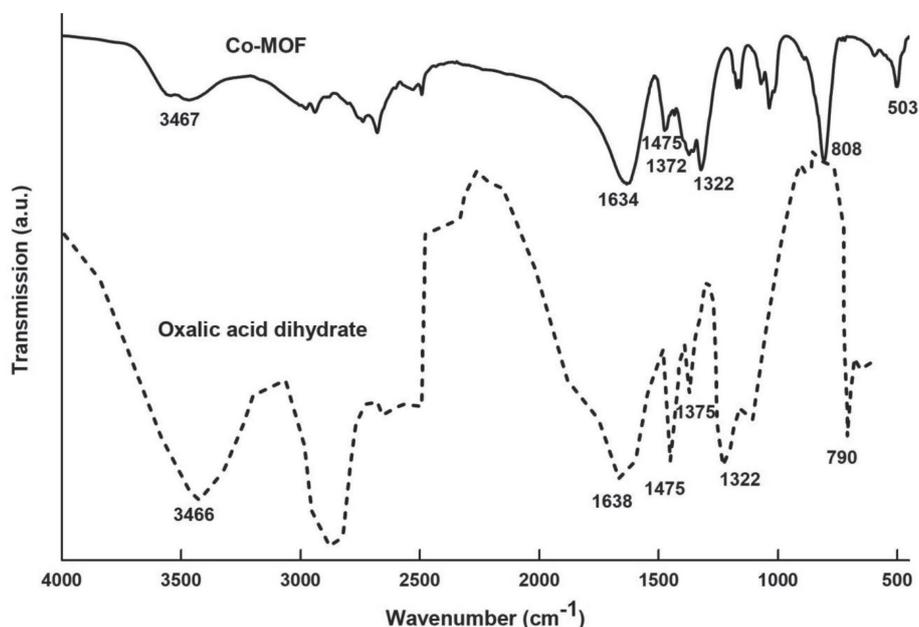

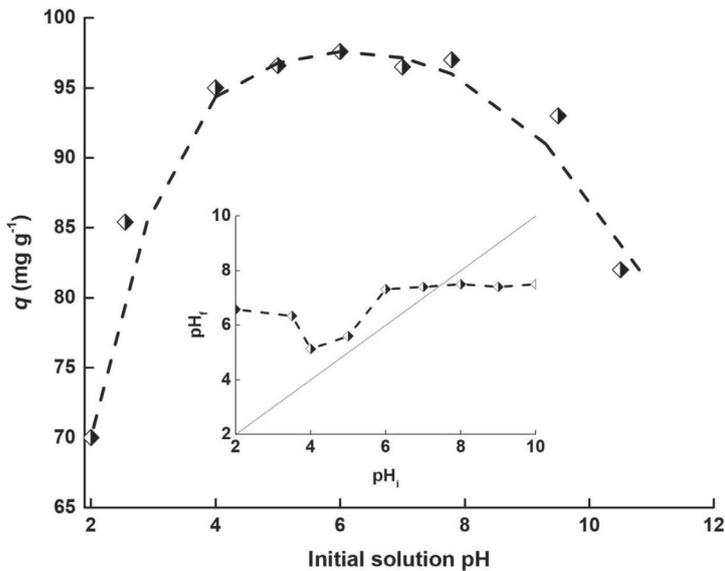Fig. 4 – *FTIR spectra of Co-MOF and oxalic acid di-hydrate*

F i g . 5 – *Effect of pH of solution on adsorption of humic acid (temperature 305 K, adsorbent dosage 25 mg, HA concentration 50 ppm); (Inset graph presents the determination of PZC of Co-MOF (temperature = 305 K, adsorbent dosage = 25 mg))*

sorbent surface and HA moieties are lower, and it can be assumed that only weak forces like Van der Waals forces play their role in the uptake of pollutant onto Co-MOF[36]. With the rise in initial solution pH, uptake of HA increased and attained a maximum value corresponding to pH 5, after which the uptake was not changing as rapidly as before until pH 7. HA contains weekly acidic, carboxylic, and phenolic functional groups, which have the tendency to ionize at mildly acidic or neutral pH. As a result, electrostatic interaction between HA and positively charged surface of Co-MOF increases the uptake. Further increase in initial solution pH from neutral to basic (above PZC 7.4) turned the adsorbent surface to negative, which led to a decline in

HA adsorption onto Co-MOF due to repulsive forces between sorbent and adsorbate. Additionally, in basic environment, HA is reported to exist in a fully dissociated form and arranged in a torus or ring-like structure, which makes it more hydrophilic and therefore less likely to adsorb on adsorbent surface[37].

Kinetics study

The results of the effect of contact time for the adsorption of HA over Co-MOF are presented in Fig. 6. It can be noticed that 90 % (~ 85 mg g^{-1}) of HA is adsorbed in less than 10 minutes and becomes slower with time. However, there is no significant change after an hour, which implies equilibrium under imposed experimental conditions. Rapid adsorption of HA in a few minutes indicates abundantly available vacant sites and high affinity between HA moieties and MOF surface. The equilibrium uptake of Co-MOF was observed to be 89 mg g^{-1}. The kinetic data was analyzed through adsorption controlled kinetic models, i.e., pseudo-first and second order kinetic models. These models consider that the formation of surface complex would be the rate-determining step in the adsorption process.

Table 2 summarizes the results of linear regression of kinetic data. Best fit model can be decided by comparing the values of some statistical parameters such as regression coefficients (R^2), and residual sum of squares (RSS). From Table 2, results show that the pseudo-second-order model is superior to first order kinetic model with high R^2 and comparatively low RSS values. Additionally, there is an insignificant difference between calculated equilibrium adsorption capacity ($q_{e,cal}$) and experimental ($q_{e,exp}$) uptake capacity for pseudo-second-or-
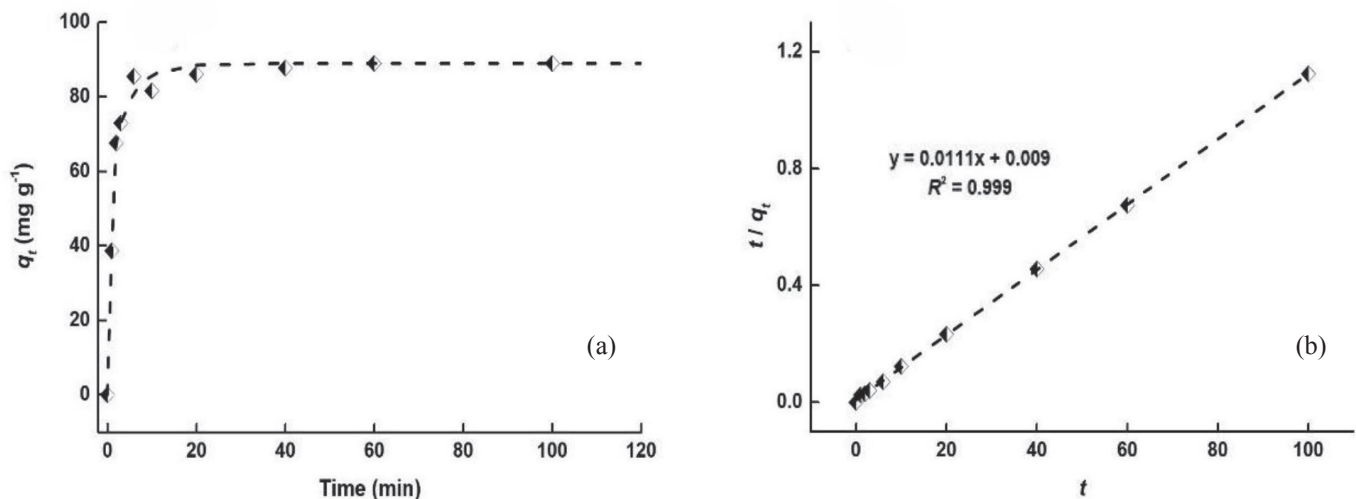

F i g . 6 – *(a) Effect of contact time on adsorption of HA onto Co-MOF (pH = 6, adsorbent dosage = 25 mg, volume = 0.05 L, HA initial concentration = 50 mg L^{-1}, temperature = 305 K) (b) pseudo-second-order plot with experimental data*

Table 2 – *Pseudo first order and pseudo second order kinetics model parameters for adsorption of HA using Co-MOF*

Parameters	Pseudo first order model (1)	Pseudo second order model (2)
$q_{e,exp}$ (mg g^{-1})	89.72	89.72
$q_{e,cal}$ (mg g^{-1})	19.44	90.57
rate constant	0.0652	0.0123
R^2	0.582	0.999
RSS	2.7034	0.0001

der model. A graphical plot based on a pseudo-second-order model can also be viewed in Fig. 6, which shows the goodness of fit kinetic data. It can be concluded that liquid film diffusion only plays its role in the adsorption of HA onto Co-MOF. The equilibrated uptake after few minutes may also be linked to depleting bulk concentration of pollutant during batch adsorption.

Adsorption isotherms

In batch adsorption, equilibrium is established between adsorbate in the solution phase with adsorbate onto Co-MOF surface at a constant temperature. Corresponding to each mentioned temperature in Fig. 7, the batch experiments were performed with different initial concentrations.

For a fixed isotherm, each data point corresponds to equilibrium concentration that was achieved for different initial concentration of the pollutant. The isotherm results follow the type III isotherm, which suggest that adsorbate-adsorbate reaction supersedes the adsorbate-adsorbent interactions. The HA uptake is low at low initial concentrations until surface coverage is sufficient, then the interactions of free and adsorbed species start to

dominate the process[38,39]. Type III isotherm can be the result of the presence of large adsorbate molecules, which are too large to access the micropores, and adsorption takes place on the surface and in extra-crystalline pores. The steepness of isotherms at higher temperature indicates that the probability of collisions among adsorbate moieties raises the adsorption capacity. Furthermore, it can be concluded that HA uptake over Co-MOF is endothermic in nature. Although the mechanism of adsorption of pollutant from aqueous phase is complicated in nature, the correlation of experimental data with theoretical isotherm models provides a clue to key mechanism steps involved in the adsorption of HA. Two-parameter isotherm models, namely Freundlich and Dubinin-Radushkevich, and three-parameter model, namely Hill and Koble-Corrigan, were used to fit the experimental data of adsorption (equations provided in Table 1).

Nonlinear regression of experimental data produced the isotherm results shown in Table 3. Freundlich isotherm equation produces fairly high correlation coefficient for all temperatures, indicating better agreement of this model equation with experimental equilibrium adsorption data of HA onto Co-MOF. K_F varies from 3.44 to 0.37 when the experimental temperature decreases from 325 K to 285 K. The parameter K_F links with adsorption capacity, and its increase with temperature reveals endothermic nature of adsorption. At all temperatures, n_F is less than one, indicating that bond energy decreases with surface density, i.e., heterogeneous nature of Co-MOF. R^2 value for DR isotherm is too low to be considered for the description of mechanism of adsorption of HA onto Co-MOF[40]. A three-parameter Hill's isotherm model produces high correlation coefficient (R^2) for all temperatures, but gives very high values of q_{max}. Apart from obtaining higher values of q_{max} from Hill isotherm, the change in up-
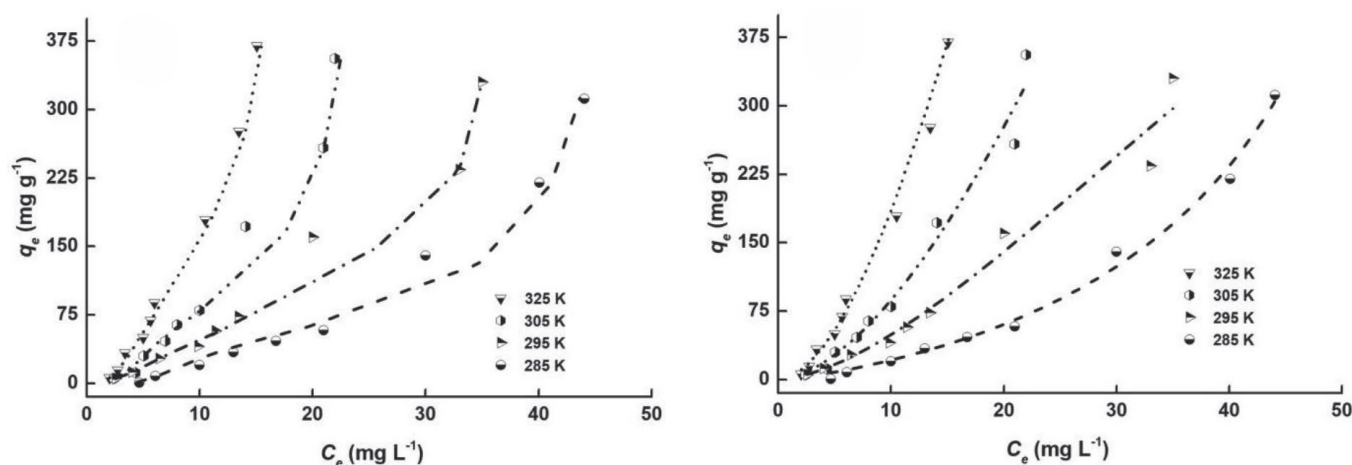

Fig. 7 – *(a) Experimental adsorption isotherms of humic acid adsorption onto Co-MOF (pH = 6, adsorbent dosage = 25 mg, volume = 0.05 L, HA initial concentration = 5–200 mg L^{-1}, temperature = 285–325 K) (b) Comparison of experimental data with KC modeled curve*

T a b l e   3 – *Parameters of isotherm models obtained from nonlinear regression for the adsorption of HA onto Co-MOF (pH = 6, adsorbent dosage = 25 mg, volume = 0.05 L, HA initial concentration = 5–200 mg L⁻¹, temperature = 285–325 K)*

Isotherm models		Temperature			
		325 K	305 K	295 K	285 K
Freundlich	K_F [(mg g⁻¹) (L mg)$^{1/n}$]	3.445	1.844	1.906	0.374
	n_F	0.579	0.598	0.703	0.568
	R^2	0.989	0.969	0.962	0.960
Dubinin-Radushkevich	q_{DR} (mg g⁻¹)	200	140	130	113
	k_{DR} (mol² kJ⁻²)	0.000003	0.000005	0.000006	0.00002
	E_d	0.408	0.316	0.288	0.158
	R^2	0.890	0.759	0.746	0.904
Hill	q_{SH} (mg g⁻¹)	3885	10116	1214	13178
	K_H (mg L⁻¹)	51.8	163.5	69.9	367.9
	n_H	1.818	1.699	1.629	1.781
	R^2	0.988	0.964	0.956	0.953
Koble Corrigan	A_{KC} (Lⁿ mg^{1-n} g⁻¹)	2.970	1.756	1.201	0.358
	B_{KC} (mg L⁻¹)	0.001	0.000	0.001	0.000
	n_{KC}	1.818	1.698	1.629	1.778
	R^2	0.988	0.964	0.956	0.953

take capacity is altogether reversed as compared to observed uptake of HA over Co-MOF. Based on the discrepancies in the results of regression of Hill isotherm equation, the model failed to describe well the adsorption results of HA. Table 3 shows that the Koble Corrigan isotherm is in good agreement with adsorption equilibrium experimental data of humic acid for all temperatures. $n_{KC} > 1$ confirms the applicability of KC isotherm model, and increase in parameter A_{KC} with temperature reveals that the adsorption of humic acid onto Co-MOF is favorable at a higher temperature. Comparison of isotherm models shows that Koble Corrigan model is the best-fitted model among all isotherms, and reveals that the surface of Co-MOF is heterogeneous. For greater visibility, the experimental data was also compared with KC model results through Fig. 7b, where it can be seen that both are in good agreement with each other.

Thermodynamic studies

Thermodynamic parameters provide an idea about the spontaneity and nature of adsorption process. These parameters include Gibbs free energy $\Delta G°$ (kJ mol⁻¹), change in enthalpy $\Delta H°$ (kJ mol⁻¹), and entropy change $\Delta S°$ (kJ mol⁻¹ K⁻¹). The pertinent equations relating to all thermodynamic pa-

rameters are summarized in Table 1. The thermodynamic equilibrium constant ($K_D = C_{ad}/C_e$), ratio of equilibrium concentration of adsorbed HA onto Co-MOF to the equilibrium concentration of HA in filtered solution) was evaluated from experimental equilibrium data. The Van't Hoff plot, i.e., ln K_D vs $1/T$, in Fig. 8, produced the values of $\Delta S°$ and $\Delta H°$; however, $\Delta G°$ was obtained from the equation provided in Table 1. The estimated values of thermodynamic parameters for adsorption of HA onto Co-MOF are listed in Table 4. The Gibbs free energy ($\Delta G°$) is negative at all temperatures, indicating that the HA adsorption process is globally spontaneous and feasible. The negativity of $\Delta G°$ increases as with temperature, implying that the adsorption of humic acid is thermodynamically favorable at a higher temperature. Positive value of $\Delta H°$ at all concentrations confirms the endothermic character of HA adsorption.

The adsorption process is usually viewed as a combination of two steps: firstly, the desorption of pre-adsorbed water molecules on the surface of Co-MOF, and secondly, the adsorption of HA species onto Co-MOF surface. In the adsorption process, HA may have to displace more than one water molecule, hence, resulting in positive values of change in enthalpy. $\Delta H°$ also helps to conclude whether the
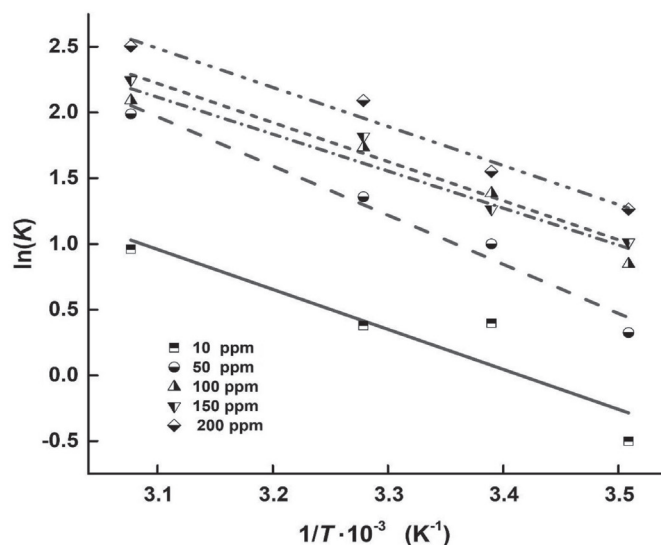
Fig. 8 – *Plot of ln(K) against 1/T for evaluation of thermodynamic parameters (25 mg Co-MOF, temperature (K): 325, 305, 295, and 285)*
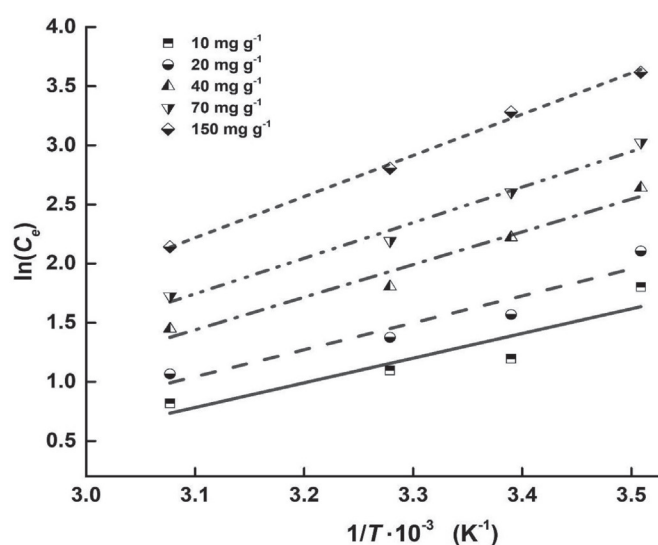

Fig. 9 – *Plot of ln(C_e) vs 1/T for the adsorption of HA on Co-MOF at constant surface coverage, q_e = 10, 20, 40, 70, 150 mg g^{-1}*

Table 4 – *Thermodynamics parameters for humic acid adsorption onto Co-MOF*

HA concentration (mg L^{-1})	$\Delta H°$ (kJ mol^{-1})	$\Delta S°$ (kJ mol^{-1} K^{-1})	$\Delta G°$ (kJ mol^{-1})			
			325 K	305 K	295 K	285 K
10	25.31±3.6	0.086±0.01	−2.778	−1.049	−0.185	0.680
50	31.10±0.7	0.113±0.002	−5.548	−3.292	−2.165	−1.037
100	23.39±1.0	0.09±0.003	−5.894	−4.092	−3.191	−2.290
150	24.75±0.7	0.095±0.002	−6.187	−4.284	−3.332	−2.380
200	24.73±1.4	0.097±0.005	−6.908	−4.961	−3.988	−3.014

adsorption mechanism is physical or chemical. If $\Delta H°$ is less than 80 kJ mol^{-1} then the adsorption can be considered as physisorption where the Van der Waal's forces and electrostatic interactions play their role in the adsorption. However, the adsorption process follows the chemisorption mechanism if $\Delta H°$ is greater than 80 kJ mol^{-1} [41]. For HA adsorption over Co-MOF, $\Delta H°$ varied in the range of 24 to 31 kJ mol^{-1}, suggesting a physisorption process. Moreover, positive value of $\Delta S°$ revealed the affinity of HA for Co-MOF, and suggested the randomness at solid/liquid interface, thereby indicating the structural variations in Co-MOF[42,43]. Overall thermodynamics parameters indicated the spontaneity, feasibility, as well as endothermicity of HA adsorption onto Co-MOF. In addition, isosteric heat of adsorption (ΔH_x) at a fixed surface coverage was calculated using Clausius-Clapeyron equation mentioned in Table 1. The isosteres related to different equilibrium adsorption capacities of HA are presented in Fig. 9. The correlation coefficients obtained through linear regression for each isostere and enthalpies of isosteres are given in Table 5. Isosteric heat of adsorption was found to be smaller than 80 kJ mol^{-1} confirming that the adsorption of

humic acid onto MOF surface involves physical forces between adsorbate and MOF. Variations in (ΔH_x) corresponding to uptake capacity of HA indicated that Co-MOF has energetically heterogeneous surface. Results revealed that (ΔH_x) increased with increase in surface coverage, probably due to the dominance of intermolecular interaction between adsorbed HA molecules. This behavior suggests the presence of possible strong lateral interaction of humic acid moieties when adsorbed on the surface of Co-MOF that already has adsorption sites of different activities. Performance of the Co-MOF to adsorb HA from aqueous phase was compared to other materials reported in the literature (Table 6). The comparison indicated reasonably good uptake of prepared Co-MOF.

Conclusion

Cobalt-based metal-organic framework (Co-MOF) was successfully synthesized by solvothermal process, and the analysis of prepared material revealed orthorhombic crystal structure of MOF. Sharp diffraction peaks in the X-ray diffractogram

Table 5 – *Isosteric enthalpies for adsorption of HA onto Co-MOF*

q_e (mg g^{-1})	ΔH_x (kJ mol^{-1})	R^2
10	17.35±3.5	0.783
20	18.93±2.3	0.877
40	22.97±1.2	0.949
70	25.02±0.5	0.978
150	28.95±0.2	0.994

Table 6 – *Comparison of adsorption capacity of Co-MOF with other reported adsorbents*

Adsorbent	Studied conditions	Adsorption capacity (mg g^{-1})	Reference
Surfactant-modified chitosan/zeolite composites (SMCZ)	pH: 7, time: 60 min, temp: 303 K, HA: (0–60 ppm), adsorbent: 25 mg	164	[34]
Surfactant-modified zeolite	time: 24 h, HA: (40–900 ppm), adsorbent: 200 mg	126	[8]
Physically and chemically treated bentonite-chitosan composite (TBCH)	pH: 4, time: 110 min, temp: 298 K, HA: (10–70 ppm), adsorbent: 70 mg	91	[35]
Cobalt-based metal-organic framework (Co-MOF)	pH: 6, time: 60 min, temp: 305 K, HA: 50 ppm, adsorbent: 25 mg	91	This study
Zeolitic Imidazole Framework-8 (ZIF-8)	time: 120 min, temp: 293 K, HA: (10–80 ppm), adsorbent: 25 mg	72	[3]
Magnetic chitosan nanoparticle (MCNP)	pH: 7, time: 60 min, temp: 298 K, HA (3–30 ppm), adsorbent: 100 mg	32.6	[12]
Zeolitic tuff	time: 48 h, HA: (700–4000 ppm), temp: 303 K, adsorbent: 1000 mg	22	[36]
Acid-treated activated carbon	time: 11 h, temp: 298 K, HA: (20 ppm), adsorbent: 25 mg	21.55	[13]
Montmorillonite nanoparticles	pH: 3, time: 15 min, temp: 298 K, HA: (40 ppm), adsorbent: 100 mg	7	[1]
Chitosan-epichlorohydrin beads	pH: 6, time: 60 min, temp: 300 K, HA: (10 ppm)	8	[37]
Fly ash	pH: 7, temp: 303 K, HA: (10–100 ppm), adsorbent: 50 mg	11	[38]
Amine-functional rice husk ash	pH: 6, time: 1 h, temp: 298 K, HA: (10–60 ppm), adsorbent: 50 mg	8	[14]

confirmed the crystal structure of MOF and Co–O bending vibrations observable in FTIR spectrum. The proposed route of using Co-MOF as a humic acid adsorbent in aqueous phase demonstrated promising results. Optimum adsorption uptake (mg g^{-1}) of humic acid on Co-MOF was attained at pH 6. The adsorption uptake increased with a rise in initial concentration and temperature of the solution of humic acid. The adsorption of humic acid obeyed pseudo-second-order kinetic model. Adsorption isotherm studies revealed that the uptake of humic acid data was well described by Koble Corrigan isotherm model, and nature of adsorption was physical as demonstrated by DR isotherm model. The negative values of $\Delta G°$, and positive values of $\Delta H°$ indicated that the HA adsorption onto Co-MOF was spontaneous, endothermic, and physical in nature. Positive change in entropy ($\Delta S°$) values revealed that the randomness increases at the adsorbate/solution interface. The isosteric heat of adsorption values confirmed that Co-MOF has heterogeneous surface. Overall, the Co-MOF is a promising adsorbent for adsorption of humic acid from the aqueous phase.

References

1. *Derakhshani, E., Naghizadeh, A.,* Optimization of humic acid removal by adsorption onto bentonite and montmorillonite nanoparticles, J. Mol. Liq. **259** (2018) 76.
doi: https://doi.org/10.1016/j.molliq.2018.03.014

2. *Abdullah, N., Rahman, M. A., Dzarfan Othman, M. H., Jaafar, J., Aziz, A. A.,* Preparation, characterizations and performance evaluations of alumina hollow fiber membrane incorporated with UiO-66 particles for humic acid removal, J. Memb. Sci. **563** (2018) 162.
doi: https://doi.org/10.1016/j.memsci.2018.05.059

3. *Lin, K. Y. A., Chang, H. A.,* Efficient adsorptive removal of humic acid from water using zeolitic imidazole framework-8 (ZIF-8), Water. Air. Soil Pollut. **226** (2015).
doi: https://doi.org/10.1007/s11270-014-2280-7

4. *Noorimotlagh, Z., Ravanbakhsh, M., Valizadeh, M. R., Bayati, B., Kyzas, G. Z., Ahmadi, M., Rahbar, N., Jaafarzadeh, N.,* Optimization and genetic programming modeling of humic acid adsorption onto prepared activated carbon and modified by multi-wall carbon nanotubes, Polyhedron **179** (2020) 114354.
doi: https://doi.org/10.1016/j.poly.2020.114354

5. *Ma, S., Liu, C., Yang, K., Lin, D.,* Coagulation removal of humic acid-stabilized carbon nanotubes from water by PACl: Influences of hydraulic condition and water chemistry, Sci. Total Environ. **439** (2012) 123.
doi: https://doi.org/10.1016/j.scitotenv.2012.09.046

6. *Rao, G., Zhang, Q., Zhao, H., Chen, J., Li, Y.,* Novel titanium dioxide/iron (III) oxide/graphene oxide photocatalytic membrane for enhanced humic acid removal from water, Chem. Eng. J. **302** (2016) 633.
doi: https://doi.org/10.1016/j.cej.2016.05.095

7. *Geng, N., Chen, W., Xu, H., Ding, M., Liu, Z., Shen, Z.,* A sono-photocatalyst for humic acid removal from water: Operational parameters, kinetics and mechanism, Ultrason. Sonochem. **57** (2019) 242.
doi: https://doi.org/10.1016/j.ultsonch.2019.03.022

8. *Li, C., Dong, Y., Wu, D., Peng, L., Kong, H.,* Surfactant modified zeolite as adsorbent for removal of humic acid from water, Appl. Clay Sci. **52** (2011) 353.
doi: https://doi.org/10.1016/j.clay.2011.03.015

9. *Zahmatkesh, M., Spanjers, H., Toran, M. J., Blánquez, P., Van Lier, J. B.,* Bioremoval of humic acid from water by white rot fungi: exploring the removal mechanisms, AMB Exp. **6** (2016).
doi: https://doi.org/10.1186/s13568-016-0293-x

10. *Chianese, S., Fenti, A., Iovino, P., Musmarra, D., Salvestrini, S.,* Sorption of organic pollutants by humic acids: A review, Mol. **25** (2020) 1.
doi: https://doi.org/10.3390/molecules25040918

11. *Wang, S., Terdkiatburana, T., Tadé, M. O.,* Single and co-adsorption of heavy metals and humic acid on fly ash, Sep. Purif. Technol. **58** (2008) 353.
doi: https://doi.org/10.1016/j.seppur.2007.05.009

12. *Dong, C., Chen, W., Liu, C.,* Preparation of novel magnetic chitosan nanoparticle and its application for removal of humic acid from aqueous solution, Appl. Surf. Sci. **292** (2014) 1067.
doi: https://doi.org/10.1016/j.apsusc.2013.12.125

13. *Eustáquio, H., Lopes, C., Da Rocha, R., Cardoso, B., Pergher, S.,* Modification of activated carbon for the adsorption of humic acid, Adsorpt. Sci. Technol. **33** (2015) 117.
doi: https://doi.org/10.1260/0263-6174.33.2.117

14. *Imyim, A., Prapalimrungsi, E.,* Humic acids removal from water by aminopropyl functionalized rice husk ash, J. Hazard. Mater. **184** (2010) 775.
doi: https://doi.org/10.1016/j.jhazmat.2010.08.108

15. *Chotzen, R. A., Polubesova, T., Chefetz, B., Mishael, Y. G.,* Adsorption of soil-derived humic acid by seven clay minerals: A systematic study, Clays Clay Min. **64** (2016) 628.
doi: https://doi.org/10.1346/CCMN.2016.064027

16. *Rowsell, J. L. C., Yaghi, O. M.,* Metal-organic frameworks: A new class of porous materials, Micro. Meso. Mater. **73** (2004) 3.
doi: https://doi.org/10.1016/j.micromeso.2004.03.034

17. *Dey, C., Kundu, T., Biswal, B. P., Mallick, A., Banerjee, R.,* Crystalline metal-Organic frameworks (MOFs): Synthesis, structure and function, Acta Crystallogr. Sect. B Struct. Sci. **70** (2014) 3.
doi: https://doi.org/10.1107/S2052520613029557

18. *Butova, V. V., Soldatov, M. A., Guda, A. A., Lomachenko, K. A., Lamberti C.,* Metal-organic frameworks: structure, properties, methods of synthesis and characterization, Russ. Chem. Rev. **85** (2016) 280.

19. *Murinzi, T. W., Hosten, E., Watkins, G. M.,* Synthesis and characterization of a cobalt-2,6-pyridinedicarboxylate MOF with potential application in electrochemical sensing, Poly. **137** (2017) 188.
doi: https://doi.org/10.1016/j.poly.2017.08.030

20. *Fan, W., Wang, Y., Xiao, Z., Huang, Z., Dai, F., Wang, R., Sun, D.,* Two-dimensional cobalt metal-organic frameworks for efficient C_3H_6/CH_4 and C_3H_8/CH_4 hydrocarbon separation, Chinese Chem. Lett. **29** (2018) 865.
doi: https://doi.org/10.1016/j.cclet.2017.11.020

21. *Nqombolo, A., Munonde, T. S., Makhetha, T. A., Moutloali, R. M., Nomngongo, P. N.,* Cobalt/zinc based metal organic frameworks as an effective adsorbent for improved removal of As(V) and Cr(VI) in a wide pH range, J. Mater. Res. Technol. **12** (2021) 1845.
doi: https://doi.org/10.1016/j.jmrt.2021.03.113

22. *Hasan, Z., Jhung, S. H.,* Removal of hazardous organics from water using metal-organic frameworks (MOFs): Plausible mechanisms for selective adsorptions, J. Hazard. Mater. **283** (2015) 329.
doi: https://doi.org/doi:10.1016/j.jhazmat.2014.09.046

23. *Feng, Y., Jiang, H., Li, S., Wang, J., Jing, X., Wang, Y., Chen, M.,* Metal-organic frameworks HKUST-1 for liquid-phase adsorption of uranium, Col. Sur. A Physicochem. Eng. Asp. **431** (2013) 87.
doi: https://doi.org/10.1016%2Fj.colsurfa.2013.04.032

24. *Nehra, M., Dilbaghi, N., Singhal, N. K., Hassan, A. A., Kim, K. H., Kumar, S.,* Metal organic frameworks MIL-100(Fe) as an efficient adsorptive material for phosphate management, Environ. Res. **169** (2019) 229.
doi: https://doi.org/10.1016/j.envres.2018.11.013

25. *Peng, Y., Huang, H., Zhang, Y., Kang, C., Chen, S., Song, L., Liu, D., Zhong, C.,* A versatile MOF-based trap for heavy metal ion capture and dispersion, Nat. Commun. **9** (2018).
doi: https://doi.org/10.1038/s41467-017-02600-2

26. *Pi, Y., Li, X., Xia, Q., Wu, J., Li, Y., Xiao, J., Li, Z.,* Adsorptive and photocatalytic removal of Persistent Organic Pollutants (POPs) in water by metal-organic frameworks (MOFs), Chem. Eng. J. **337** (2018) 351.
doi: https://doi.org/10.1016/j.cej.2017.12.092

27. *Zhang, S., Wang, J., Zhang, Y., Ma, J., Huang, L., Yu, S., Chen, L., Song, G., Qiu, M., Wang, X.,* Applications of water-stable metal-organic frameworks in the removal of water pollutants: A review, Environ. Pol. **291** (2021) 118076.
doi: https://doi.org/10.1016/j.envpol.2021.118076

28. *Zhao, X., Wang, T., Du, G., Zheng, M., Liu, S., Zhang, Z., Zhang, Y., Gao, X., Gao, Z.,* Effective removal of humic acid from aqueous solution in an Al-based metal-organic framework, J. Chem. Eng. Data **64** (2019) 3624.
doi: https://doi.org/10.1021/acs.jced.9b00387

29. *Oveisi, M., Asli, M. A., Mahmoodi, N. M.*, MIL-Ti metal-organic frameworks (MOFs) nanomaterials as superior adsorbents: Synthesis and ultrasound-aided dye adsorption from multicomponent wastewater systems, J. Haz. Mater. **347** (2018) 123.
doi: https://doi.org/10.1016/j.jhazmat.2017.12.057

30. *Zahir, A., Aslam, Z., Aslam, U., Abdullah, A., Ali, R., Bello, M. M.*, Paspalum notatum grass-waste-based adsorbent for rhodamine B removal from polluted water, Chem. Biochem. Eng. *Q.* **34** (2020) 93.
doi: https://doi.org/10.15255/CABEQ.2020.1830

31. *Rehman, M. Z. Ur, Aslam, Z., Shawabkeh, R. A., Hussein, I. A., Mahmood, N.*, Concurrent adsorption of cationic and anionic dyes from environmental water on amine functionalized carbon, Water Sci. Technol. **81** (2020) 466.
doi: https://doi.org/10.2166/wst.2020.119

32. *Samiullah, M., Aslam, Z., Rana, A. G., Abbas, A., Ahmad, W.*, Alkali-activated boiler fly ash for Ni(II) removal: Characterization and parametric study, Water. Air. Soil Pol. **229** (2018).
doi: https://doi.org/10.1007/s11270-018-3758-5

33. *Qian, J., Sun, F., Qin, L.*, Hydrothermal synthesis of zeolitic imidazolate framework-67 (ZIF-67) nanocrystals, Mater. Lett. **82** (2012) 220.
doi: https://doi.org/10.1016/j.matlet.2012.05.077

34. *Thakkar, H., Eastman, S., Al-Naddaf, Q., Rownaghi, A. A., Rezaei, F.*, 3D-Printed metal-organic framework monoliths for gas adsorption processes, ACS Appl. Mater. Inter. **9** (2017) 35908.

35. *Thornton, D. A.*, Metal complexes of aniline: Infrared and raman spectra, J. Coord. Chem. **24** (1991) 261.
doi: https://doi.org/10.1080/00958979109407887

36. *Bouras, H. D., Benturki, O., Bouras, N., Attou, M., Donnot, A., Merlin, A., Addoun, F., Holtz, M. D.*, The use of an agricultural waste material from *Ziziphus jujuba* as a novel adsorbent for humic acid removal from aqueous solutions, J. Mol. Liq. **211** (2015) 1039.
doi: https://doi.org/10.1016/j.molliq.2015.08.028

37. *Anirudhan, T. S., Suchithra, P. S., Rijith, S.*, Amine-modified polyacrylamide-bentonite composite for the adsorption of humic acid in aqueous solutions, Col. Surf. A Physicochem. Eng. Asp. **326** (2008) 147.
doi: https://doi.org/10.1016/j.colsurfa.2008.05.022

38. *Thommes, M., Kaneko, K., Neimark, A. V., Olivier, J. P., Rodriguez-Reinoso, F., Rouquerol, J., Sing, K. S. W.*, Physisorption of gases, with special reference to the evaluation of surface area and pore size distribution (IUPAC Technical Report), Pure Appl. Chem. **87** (2015) 1051.
doi: https://doi.org/10.1515/pac-2014-1117

39. *De Smedt, C., Ferrer F., Leus, K., Spanoghe, P.,* Removal of pesticides from aqueous solutions by adsorption on zeolites as solid adsorbents, Adsorpt. Sci. Technol. **33** (2015) 457.

40. *Özcan, A., Özcan, A. S., Tunali, S., Akar, T., Kiran, I.*, Determination of the equilibrium, kinetic and thermodynamic parameters of adsorption of copper(II) ions onto seeds of *Capsicum annuum*, J. Hazard. Mater. **124** (2005) 200.
doi: https://doi.org/10.1016/j.jhazmat.2005.05.007

41. *Bouhamidi, Y., Kaouah, F., Nouri, L., Boumaza, S., Trari, M., Bendjama, Z.*, Kinetic, thermodynamic, and isosteric heat of dibutyl and diethyl phthalate removal onto activated carbon from *Albizzia julibrissin* pods, Part. Sci. Technol. **36** (2018) 235.
doi: https://doi.org/10.1080/02726351.2016.1243179

42. *Darwish, A. A. A., Rashad, M., AL-Aoh, H. A.,* Methyl orange adsorption comparison on nanoparticles: Isotherm, kinetics, and thermodynamic studies, Dye. Pig. **160** (2019) 563.
doi: https://doi.org/10.1016/j.dyepig.2018.08.045

43. *Doulia, D., Leodopoulos, C., Gimouhopoulos, K., Rigas, F.*, Adsorption of humic acid on acid-activated Greek bentonite, J. Col. Inter. Sci. **340** (2009) 131.
doi: https://doi.org/10.1016/j.jcis.2009.07.028